MASTER'S THESIS

Master of Science in Advanced Mathematics and Mathematical Engineering

Title: Dynamics of crack propagation with adaptive refinement based on unfitted meshes

Author: Adrià Pons Puntí

Advisors: Sonia Fernández-Méndez & Alba Muixí Ballonga

Department: Department of Civil and Environmental Engineering

Academic year: 2019-2020

UNIVERSITAT POLITÈCNICA DE CATALUNYA
BARCELONATECH
Facultat de Matemàtiques i Estadística

Universitat Politècnica de Catalunya
Facultat de Matemàtiques i Estadística

Master in Advanced Mathematics and Mathematical Engineering

Master's thesis

Dynamics of crack propagation with adaptive refinement based on unfitted meshes

Adrià Pons Puntí

Supervised by Sonia Fernández-Méndez & Alba Muixí

June, 2020

To carry out this project I have had the help of some people, without whose support the whole study could not have been possible. That is why I would like to thank:

- All my family, especially my parents, my brother and my grandmother, for all the advice they have given me.

- My friends David and Gerard, for their help in some parts of the project, and Marta and Nora, for helping me with the review.

- Lastly, my advisors Sonia and Alba, for all the hours they have spent on the project and the enormous help they have given me. I would also like to give a special thank-you to professor Antonio Rodríguez for joining our meetings and helping us interpreting some of the results.

Abstract

Fracture mechanics is a field of mechanics concerned with the study of the propagation of cracks originated in different materials. This field has achieved great popularity in recent years, due to the massive interest of engineers to understand and predict the behaviour of various materials when they are subjected to different forces, such as traction or compression. In this project we consider one of the most used models in this area: phase-field models. These models require very fine meshes along crack paths. This work applies an automatic adaptive Finite Element method, based on Nitsche's method, to the solution of transient problems.

Keywords

Numerical methods, PDEs, Phase-Field, Fracture, Crack, Linear elasticity, Branching

Contents

1. Introduction

Fracture mechanics is a field of mechanics concerned with the study of the propagation of cracks (or fractures) originated in different materials. This field has achieved great popularity in recent years, due to the massive interest of engineers to understand and predict the behaviour of various materials when they are subjected to different forces, such as traction or compression.

There are two main ways of modelling these cracks or fractures: discontinuous and continuous descriptions. The first describe the crack using discontinuous displacement fields and, although it might be used due to its simplicity, there is not an accurate strategy to determine the fracture direction at each time step. Moreover, the remeshing needed to capture the solution at each time step makes it computationally inefficient. Continuous descriptions, however, describe the crack with a damaged zone that has lost its carrying capacity. Using this approach, the mesh does not have to be adapted to the crack and, thus, there is no need for a remeshing at each time step, although we need the mesh to be finer on the path we expect the crack to follow.

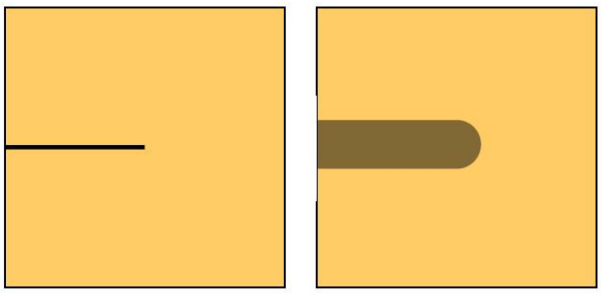

Figure 1: On the left, crack represented by a discontinuous model. On the right, damage zone of a continuous model. Figure from [5].

There mainly exist two divisions inside the continuous models: phase-field models and gradient-damage models. In this thesis we are going to focus on phase-fields models, which are given by an energetic formulation that we are going to discuss later on. These models can be quasi-static or dynamic, being the later the ones that we are going to treat.

This project intends to be the natural continuation of the following degree theses: in [8], a first approach to continuous models is done, comparing phase-field and gradient-damage quasi-static models in order to determine their similarities and differences. In [2], the study is focused just on phase-field dynamic models. The main challenge of the later is the difficulty of knowing beforehand the path the crack is going to take in each example and, thus, where to refine our mesh. To do so, the author of the thesis refined the mesh by hand during the computations in order to obtain the desired refined mesh for the specific treated example.

This thesis will try to solve this difficulty by implementing a routine that will automatically refine the mesh when the damaged zone approaches a new element. This will be done following the technique proposed for the quasi-static problem in [6], taking advantage of the code that the author, Alba Muixí, used for the quasi-static phase-field model and adapting it to solve the dynamic problem.

1.1 Thesis structure

The main goal of this thesis is to solve the dynamic phase-field model using an adaptive refinement that will allow us to work on different scenarios without having to refine the mesh manually for each example. To do so, we are going to start by recalling the dynamic phase-field model using an energetic formulation. Then, we are going to explain the two equations that are part of the model, as well as how to solve them, and the automatic adaptive refinement technique based on Nitsche's method. Finally, we are going to test our code with some examples and we will show how the parameters of the model affect the final result.

Let us remark that in the whole project we consider a domain $\Omega \subset \mathbb{R}^2$. All methods and routines of this thesis have been coded in *Matlab*, based on the code that Alba Muixí used in [6] for the quasi-static phase-field model. In order to make all calculations in a reasonable time window, most of the computations have been sent to *Clonetroop*, a cluster used for serial or parallel scientific calculations located in the *Laboratori de Càlcul Numèric de la UPC*.

2. Dynamic phase-field model

Let $\Omega \subset \mathbb{R}^2$ be a body with an internal discontinuity on Γ_c, the material's crack. We consider a phase-field model, based on an energetic formulation of the problem. Under deformation, cracks are assumed to propagate along the path of least energy. This energy can be expressed as the sum of the elastic deformation energy and the crack generation energy, that is,

$$E(\mathbf{u}) = \int_{\Omega} \Psi(\varepsilon)\, d\Omega + G_c \int_{\Gamma_c} d\Gamma_c\,, \tag{1}$$

where G_c is the critical energy release rate, a value that, when reached, allows the crack to move forward, and Ψ is the elastic energy density, being ε the deformations. In our project we are going to consider homogeneous isotropic lineal elastic materials, so stresses σ_{ij} and deformations ε_{ij} are related by

$$\sigma_{ij} = \sum_{k,l} \mathcal{C}_{ijkl}\, \varepsilon_{ij}\,,$$

where $\boldsymbol{\mathcal{C}}$ is a fourth order elasticity tensor that depends on two Lamé material parameters: λ and μ. These parameters are related to the Young's modulus E and the Poisson ratio ν, that are going to be used further in this work. Under these hypothesis, we also have that the elastic energy density is given by $\Psi(\varepsilon) = \varepsilon : \boldsymbol{\mathcal{C}} : \varepsilon$, where the small deformation tensor ε is defined by $\varepsilon(\mathbf{u}) = (\nabla \mathbf{u} + \nabla \mathbf{u}^T)/2$.

In phase-field models, a smoothed representation of the fracture is introduced in order to help numerical computations. That is, to model the smooth transition between unbroken and broken states of the material, an auxiliary field d is introduced in the formulation. The field d is called phase-field variable or damage variable and it varies smoothly between two values representing both states, usually 0 for undamaged and 1 for completely broken (see figure 2).

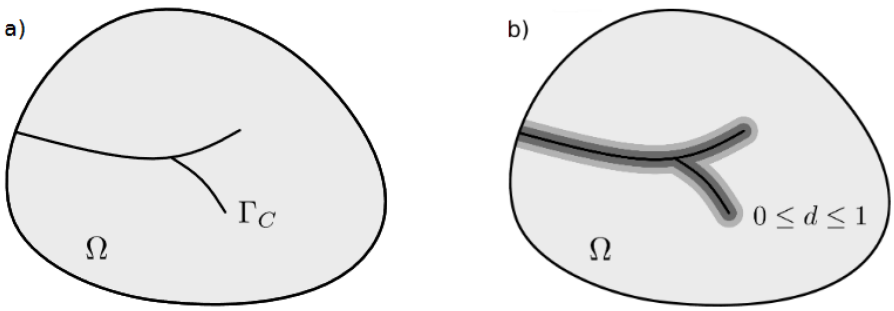

Figure 2: (a) Body with a crack Γ_C. (b) Body with a diffuse band due to the introduction of variable d. Figure from [7].

Based on the fracture theory that can be seen in [1], the total energy of a material in a domain Ω (1)

can be approximated as

$$E(\mathbf{u}, d) = \int_\Omega (1-d)^2 \Psi(\varepsilon)\, d\Omega + G_c \int_\Omega \left(\frac{d^2}{2l} + \frac{l}{2} |\nabla d|^2 \right) d\Omega\,, \tag{2}$$

where l is a variable that controls the crack's width.

Minimising (2) we obtain the system of equations that we need to solve for the displacements $\mathbf{u}$ and the phase-field variable d:

$$\begin{cases} \rho \ddot{\mathbf{u}} = \nabla \cdot \boldsymbol{\sigma}\,, & \text{(3a)} \\ \boldsymbol{\sigma}(\mathbf{u}, d) = (1-d)^2 \dfrac{\partial \Psi(\varepsilon)}{\partial \varepsilon}\,, \qquad \text{(Constitutive Equation)} & \text{(3b)} \\ -l^2 \Delta d + d = \dfrac{2l}{G_c}(1-d)\mathcal{H}(\mathbf{u})\,, & \text{(3c)} \end{cases}$$

where

$$\ddot{\mathbf{u}} = \frac{d^2\mathbf{u}}{dt^2} \qquad \text{and} \qquad \frac{\partial \Psi(\varepsilon)}{\partial \varepsilon} = \boldsymbol{\mathcal{C}} : \varepsilon(\mathbf{u})\,.$$

It is also important to note that in the last equation a new variable $\mathcal{H}$ appears, computed as $\mathcal{H}(\mathbf{u}) = \max_{\tau \in [0,t]} \Psi(\varepsilon(\mathbf{u}))$. It is a history field and its basic role is to make the crack irreversible. See [4] for more information about it.

Given the solution at a time n, the solution at time $n+1 = n + \Delta t$ is computed solving the system (3) with boundary conditions

$$\begin{cases} \mathbf{u} = \mathbf{u}_D^{n+1} & \text{on } \Gamma_D\,, & \text{(4a)} \\ \boldsymbol{\sigma}(\mathbf{u}, d) \cdot \mathbf{n} = \mathbf{t}_N^{n+1} & \text{on } \Gamma_N\,, & \text{(4b)} \\ \nabla d \cdot \mathbf{n} = 0 & \text{on } \partial\Omega\,, & \text{(4c)} \end{cases}$$

where $\mathbf{u}_D^{n+1}$ and $\mathbf{t}_N^{n+1}$ are the prescribed displacements and tractions, respectively, and $\mathbf{n}$ is the outward unit normal to the boundary. Γ_D and Γ_N stand for the Dirichlet and Neumann boundaries for the equilibrium equation, satisfying $\Gamma_D \cap \Gamma_N = \emptyset$ and $\partial\Omega = \Gamma_D \cup \Gamma_N$.

System (3) with boundary conditions (4) is solved in a decoupled way. In each time step the displacement $\mathbf{u}^{n+1}$ is computed, solving (3a) with (3b), (4a) and (4b), assuming $d = d^n$. Then, the damage is updated computing d^{n+1} as solution of (3c) with (4c) and $\mathbf{u} = \mathbf{u}^{n+1}$.

3. Refinement strategy. Nitsche's method

Phase-field models need more resolution near cracks, since the displacement and damage fields present sharp variations. As cracks propagate, the space of approximation has to be accordingly refined to obtain a good representation of the solution. In order to do that, we are going to take into account the following concepts, proposed in [6] in the context of quasistatic problems.

i. We are going to use two types of elements with different approximation spaces, called *standard* and *refined*. Standard elements are mapped to the standard reference element, whose space of approximation is the space of polynomials up to degree p, while refined elements are mapped to the refined reference element, whose space of approximation is h-refined with a uniform submesh with $m^{n_{sd}}$ subelements, for a given refinement factor m and spatial dimension n_{sd}.

ii. The refinement factor m is going to be fixed, known a priori and depending on the length-scale l of the model.

iii. We will impose a weak continuity on the interface between refined and standard elements by means of Nitsche's method.

Note that the computational mesh is fixed during all the simulation. Elements along cracks are refined, while the rest of the elements of the mesh are assumed as standard. As the simulation evolves and cracks propagate, more elements become refined. The indicator that is going to be used to determine whether an element needs to be refined or not is the damage field d. More precisely, we are going to refine an element if the value of d in any of its nodes is greater than 0.2, since it has been observed that with this threshold results are accurate and robust. This refining criterion is applied at each time step.

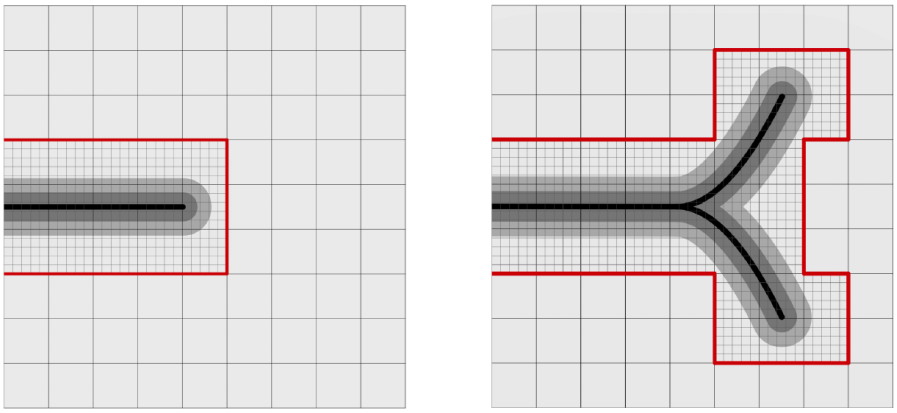

Figure 3: Cartoon of a discretization in two consecutive steps, with standard and refined elements. In red, interface in which continuity is imposed in weak form. Figure from [6].

As aforementioned, we are going to impose continuity on the interface in weak form (in red in Figure 3). That is because, if imposed in strong form, finding the relations between nodes for an arbitrary refinement factor m may be cumbersome in practice. In this thesis we will use Nitsche's method to weakly impose continuity. To do so we are going to define some concepts that will be useful:

i. We will use two subdomains Ω_1 and Ω_2, satisfying $\bar{\Omega} = \bar{\Omega}_1 \cup \bar{\Omega}_2$ and $\Omega_1 \cap \Omega_2 = \emptyset$. Ω_1 will be covered by standard elements and Ω_2 by refined elements.

ii. The interface where the continuity is going to be imposed is defined as $\Gamma = \partial\Omega_1 \cap \partial\Omega_2$.

iii. We define the functional space

$$\mathcal{V}(\Omega) = \{v \in L^2(\Omega) : v|_{\Omega_i} \in H^1(\Omega_i), \text{ for } i = 1, 2\},$$

including discontinuous functions across Γ.

iv. We define two operators: the mean $\{\odot\} = \frac{1}{2}(\odot_1 + \odot_2)$, and the jump $[\![\odot]\!] = \odot_1 \mathbf{n}_1 + \odot_2 \mathbf{n}_2 = (\odot_1 - \odot_2)\mathbf{n}_1$, where $\mathbf{n}_1, \mathbf{n}_2$ stand for the unit exterior normals to Ω_1 and Ω_2. Also, lower indices 1 and 2 in functions indicate their values on Γ from Ω_1 and Ω_2, respectively.

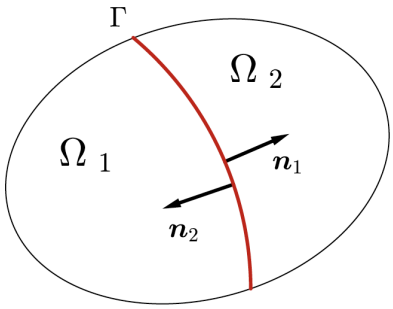

Figure 4: Adjacent domains Ω_1 and Ω_2. Continuity is imposed by Nitsche's method on Γ (in red). Figure from [6].

Nitsche's method is going to be used in both the equilibrium and the damage equations, that together form the phase-field system (3). In the following subsections we are going to study each equation and how Nitsche's method is used in their formulation.

3.1 Equilibrium equation

The equilibrium equation in (3) can be rewritten in the broken domain Ω as

$$\begin{cases} \rho\ddot{\mathbf{u}} = \nabla \cdot \boldsymbol{\sigma} & \text{in } \Omega = \Omega_1 \cup \Omega_2, \\ \boldsymbol{\sigma} = (1-d)^2 \mathcal{C} : \varepsilon(\mathbf{u}) & \\ \mathbf{u}^0 = 0 & \text{in } \Omega, \\ \dot{\mathbf{u}}^0 = 0 & \text{in } \Omega, \\ \mathbf{u} = \mathbf{u}_D & \text{on } \Gamma_D, \\ \boldsymbol{\sigma}(\mathbf{u}) \cdot \mathbf{n} = \mathbf{t}_N & \text{on } \Gamma_N, \\ [\![\mathbf{u} \otimes \mathbf{n}]\!] = 0 & \text{on } \Gamma, \\ [\![\boldsymbol{\sigma}(\mathbf{u}) \cdot \mathbf{n}]\!] = 0 & \text{on } \Gamma, \end{cases} \tag{5}$$

where the first two equations are the equilibrium equation with its constitutive equation, complemented with the following four expressions, the initial conditions and the usual boundary conditions. The second-to-last equation ensures continuity of displacements and the last one, the equilibrium of tractions.

The strategy to derive the formulation (Nitsche's method) consists on writing the standard finite element weak form (see appendix A) for each one of the subdomains Ω_1 and Ω_2, and summing them up. So we need to find $\mathbf{u} \in [\mathcal{V}(\Omega)]^{n_{sd}}$ such that

$$\int_\Omega \rho \mathbf{v} \cdot \ddot{\mathbf{u}} \, d\Omega = \int_{\Gamma_N} \mathbf{v} \cdot \mathbf{t}_N \, ds + \int_\Gamma \mathbf{v}_1 \cdot \boldsymbol{\sigma}(\mathbf{u}_1) \cdot \mathbf{n}_1 + \mathbf{v}_2 \cdot \boldsymbol{\sigma}(\mathbf{u}_2) \cdot \mathbf{n}_2 \, ds - \int_\Omega \nabla \mathbf{v} : \boldsymbol{\sigma}(\mathbf{u}) \, d\Omega \,, \tag{6}$$

for all $\mathbf{v}$ such that $\mathbf{v} = \mathbf{0}$ on Γ_D. Rearranging the second integral of the right hand side of (6) by using the algebraic identity $\mathbf{a}_1 \cdot \mathbf{b}_1 \cdot \mathbf{n}_1 + \mathbf{a}_2 \cdot \mathbf{b}_2 \cdot \mathbf{n}_2 = \{\mathbf{a}\} \cdot [\![\mathbf{b} \cdot \mathbf{n}]\!] + [\![\mathbf{a} \otimes \mathbf{n}]\!] : \{\mathbf{b}\}$ and using the last condition of (5), we obtain the expression

$$\int_\Omega \rho \mathbf{v} \cdot \ddot{\mathbf{u}} \, d\Omega = \int_{\Gamma_N} \mathbf{v} \cdot \mathbf{t}_N \, ds + \int_\Gamma [\![\mathbf{v} \otimes \mathbf{n}]\!] : \{\boldsymbol{\sigma}(\mathbf{u})\} \, ds - \int_\Omega \nabla \mathbf{v} : \boldsymbol{\sigma}(\mathbf{u}) \, d\Omega \,. \tag{7}$$

At this point, the resulting bilinear form is neither symmetric nor coercive. To fix this, we introduce two consistent (i.e., null) integrals thanks to the continuity of displacements, i.e. second-to-last equation in (5). Thus, using Nitsche's method, the equilibrium equation's weak form is: find $\mathbf{u}$ such that $\mathbf{u}(\cdot, t) \in [\mathcal{V}(\Omega)]^{n_{sd}} \, \forall t$ and

$$\begin{aligned} \int_\Omega \rho \mathbf{v} \cdot \ddot{\mathbf{u}} \, d\Omega = \int_{\Gamma_N} \mathbf{v} \cdot \mathbf{t}_N \, ds + \int_\Gamma [\![\mathbf{v} \otimes \mathbf{n}]\!] : \{\boldsymbol{\sigma}(\mathbf{u})\} \, ds + \int_\Gamma \{\boldsymbol{\sigma}(\mathbf{v})\} : [\![\mathbf{u} \otimes \mathbf{n}]\!] \, ds \\ - \beta_E \int_\Gamma [\![\mathbf{u} \otimes \mathbf{n}]\!] : [\![\mathbf{v} \otimes \mathbf{n}]\!] \, ds - \int_\Omega \nabla \mathbf{v} : \boldsymbol{\sigma}(\mathbf{u}) \, d\Omega \,, \end{aligned} \tag{8}$$

with the initial conditions

$$\begin{cases} \mathbf{u}^0 = 0 & \text{in } \Omega \,, \\ \dot{\mathbf{u}}^0 = 0 & \text{in } \Omega \,, \end{cases}$$

for all $\mathbf{v}$ such that $\mathbf{v}(\cdot, t) \in [\mathcal{V}(\Omega)]^{n_{sd}} \, \forall t$ and $\mathbf{v} = \mathbf{0}$ on Γ_D. The third integral of the right hand side of (8) makes the functional symmetric, while the fourth one ensures coercivity of the bilinear form for a large enough value of the positive scalar constant β_E. This parameter is key for the stability of the formulation. We can take the parameter of the form

$$\beta_E = \alpha_E E (h/m)^{-1} \,,$$

where E is the Young's modulus, h denotes the element size in the background mesh and m stands for the refinement factor. Taking this relation into account, the parameter that we tune is α_E, called Nitsche's parameter, that needs to be large enough. For the entire project we are going to take $\alpha_E = 100$.

Nitsche's formulation is very robust in terms of the aforementioned parameter. Moderate values of α_E are enough to ensure stability of the solution and there is a wide interval of proper values. When its value is not large enough, solutions are clearly wrong and the unstabilities can be appreciated at plain sight. Going to the other extreme, for values of α_E which are much larger than the minimum value providing coercivity, the matrix becomes ill-conditioned.

The code from Alba Muixí based on [6] implements the aforementioned method for the quasi-static equation, that is, not taking into account the temporal derivative. For this project, we have taken Alba's code and adapted it in order to include the dynamic part. Thus, after discretizing the weak form (8) we will obtain a system of linear ODEs

$$\mathbf{M}\ddot{\mathbf{U}} + \mathbf{K}\mathbf{U} = \mathbf{f}\,, \tag{9}$$

where $\mathbf{K}$ and $\mathbf{f}$ are the matrix and the vector corresponding to the discretization of the quasi-static problem, already implemented in Alba's code. We define $\mathbf{M}$ using the basis functions N_i as

$$\mathbf{M} = \begin{bmatrix} \hat{\mathbf{M}} & & \\ & \hat{\mathbf{M}} & \\ & & \end{bmatrix}, \quad \text{with} \quad \hat{m}_{ij} = \int_\Omega \rho N_i N_j \, d\Omega\,.$$

Newmark method

In order to solve the linear system of ODEs (9) we are going to use the so-called Newmark's method, a method of numerical integration widely used in computation dynamics.

We will denote as Δt the fixed time step. Given the solution at $t^n = n\Delta t$, i.e. $\mathbf{U}^n$, $\dot{\mathbf{U}}^n$ and $\ddot{\mathbf{U}}^n$, we calculate $\mathbf{U}^{n+1}$ and $\dot{\mathbf{U}}^{n+1}$ by means of generalised Taylor series,

$$\begin{aligned} \mathbf{U}^{n+1} &= \mathbf{U}^n + \Delta t \dot{\mathbf{U}}^n + \Delta t^2 \left(\left(\frac{1}{2} - \beta \right) \ddot{\mathbf{U}}^n + \beta \ddot{\mathbf{U}}^{n+1} \right), \\ \dot{\mathbf{U}}^{n+1} &= \dot{\mathbf{U}}^n + \Delta t \Big((1-\gamma) \ddot{\mathbf{U}}^n + \gamma \ddot{\mathbf{U}}^{n+1} \Big), \end{aligned} \tag{10}$$

where β and γ are two parameters such that $0 \leq \beta \leq 1/2$ and $0 \leq \gamma \leq 1$. Note that, for $\beta = \gamma = 0$, we recover the usual Taylor series.

Now, we impose equilibrium at time t^{n+1} for

$$\mathbf{M}\ddot{\mathbf{U}}^{n+1} + \mathbf{K}\mathbf{U}^{n+1} = \mathbf{f}^{n+1}\,. \tag{11}$$

Substituting $\mathbf{U}^{n+1}$ and $\dot{\mathbf{U}}^{n+1}$ using (10), we get the system of equations for $\ddot{\mathbf{U}}^{n+1}$

$$\Big(\mathbf{M} + \Delta t^2 \beta \mathbf{K}\Big)\ddot{\mathbf{U}}^{n+1} = \mathbf{f}^{n+1} - \mathbf{K}\left(\mathbf{U}^n + \Delta t \dot{\mathbf{U}}^n + \left(\frac{1}{2} - \beta\right)\Delta t^2 \ddot{\mathbf{U}}^n\right). \tag{12}$$

So, in order to solve our system of ODEs (9), given the solution at t^n, we solve the linear system (12) to compute the accelerations $\ddot{\mathbf{U}}^{n+1}$. Then, we use them to compute the displacements $\mathbf{U}^{n+1}$ and velocities $\dot{\mathbf{U}}^{n+1}$ by means of (10). Note that, in the whole project, we are going to take $\beta = 1/4$ and $\gamma = 1/2$, since they guarantee unconditional stability for any time step Δt, and the convergence will be of the order $\mathcal{O}(\Delta t^2)$.

We have implemented a code in `Matlab` that solves the dynamic equilibrium equation and now we aim to do some testing. We consider a squared domain $\Omega = [-1, 1]^2$ with linear standard elements of size $h = 2^{-3}$. We refine those elements within $[-1, 1] \times [-1, 0]$ with a refinement factor $m = 3$ and solve the system

$$\begin{cases} \rho \ddot{\mathbf{u}} = \nabla \cdot \boldsymbol{\sigma} + \rho \mathbf{b}\,, \\ \boldsymbol{\sigma}(\mathbf{u}, d) = (1 - d)^2 \boldsymbol{\mathcal{C}} : \varepsilon(\mathbf{u})\,, \end{cases} \tag{13}$$

where we compute the external forces $\mathbf{b}$ so that we obtain a certain analytical solution. More precisely, we consider the analytical solution to be

$$u_x = \sin(x + y)\,, \qquad u_y = x^2 + y^2\,. \tag{14}$$

Taking $\rho = 1$, $d = 0$, $E = 1$ and $\nu = 0.2$, we integrate the system until $t = 1\,s$ with a time step of $\Delta t = 10^{-3}$. We impose Dirichlet boundary conditions in the whole boundary so that we obtain the analytical solution (14).

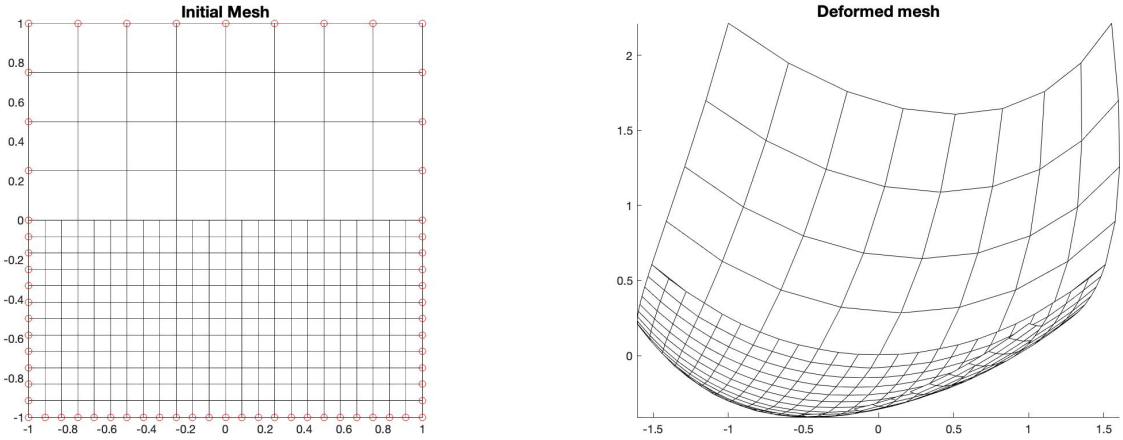

(a) Initial square mesh.

(b) Deformed mesh after applying the equilibrium equation.

Figure 5: Deformation of a square mesh using the analytical solution (14).

The next step is to make a convergence plot. That is, to compute the L_2 norm between the analytical and the obtained solutions for different element sizes h and different mesh element degrees p. As it can be seen on the following picture, the straight lines have an approximate slope of $p+1$ and, thus, the method behaves as expected.

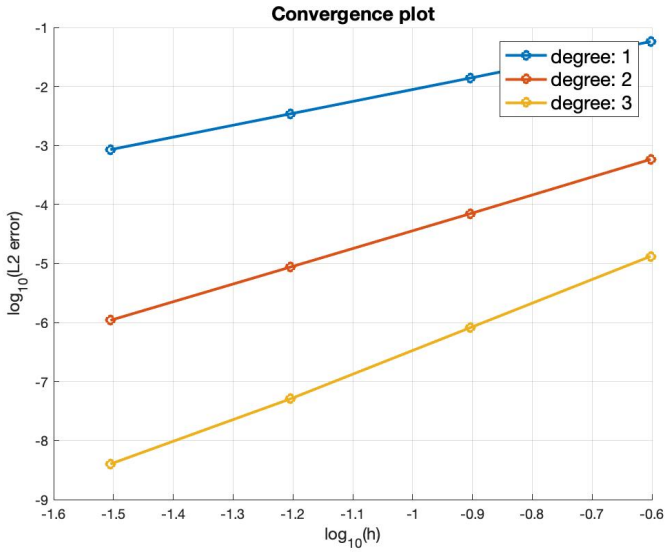

DEGREE	SLOPE
1	2.03
2	3.02
3	3.91

Figure 6: Convergence plot with the slopes of the three straight lines.

3.2 Damage equation

As we did with the equilibrium equation, the damage equation in (3) can be also rewritten in the broken domain Ω as

$$\begin{cases} -l^2\Delta d + d = \dfrac{2l}{Gc}(1-d)\mathcal{H} & \text{in } \Omega = \Omega_1 \cup \Omega_2\,, \\ \nabla d \cdot \mathbf{n} = 0 & \text{on } \Gamma_N = \partial\Omega\,, \\ [\![d\mathbf{n}]\!] = 0 & \text{on } \Gamma\,, \\ [\![\nabla d \cdot \mathbf{n}]\!] = 0 & \text{on } \Gamma\,, \end{cases} \tag{15}$$

where the first two equations are the damage equation with its boundary condition, and the last two, as with the equilibrium equation, impose continuity of the damage field and its normal derivative on the interface Γ.

Again, we are going to use Nitsche's method, so we are going to add the weak form of the damage equation (see appendix B) on both subdomains Ω_1 and Ω_2. Then, we will add two consistent integrals as we did with the equilibrium equation, in order to obtain a symmetric and coercive bilinear form. So, to sum up, we need to find $d \in \mathcal{V}(\Omega)$ such that

$$\begin{aligned} \int_\Omega \left(\frac{Gc}{l} + 2\mathcal{H}\right) v d \, d\Omega + \int_\Omega G_c l \nabla v \cdot \nabla d \, d\Omega - \int_\Gamma G_c l [\![v\mathbf{n}]\!] \cdot \{\nabla d\} \, ds \\ - \int_\Gamma G_c l [\![d\mathbf{n}]\!] \cdot \{\nabla v\} \, ds + \beta_D \int_\Gamma [\![d\mathbf{n}]\!] \cdot [\![v\mathbf{n}]\!] \, ds = \int_\Omega v 2\mathcal{H} \, d\Omega\,, \end{aligned} \tag{16}$$

for all $v \in \mathcal{V}(\Omega)$. As it happened with the equilibrium equation, in this case we also have a parameter β_D that ensures the coercivity of the bilinear form. To obtain optimal convergence, this parameter can be taken as

$$\beta_D = \alpha_D G_c l (h/m)^{-1}\,,$$

with α_D the parameter that we need to tune. For the entire project we are going to take $\alpha_D = 100$.

Discretizing the weak form (16) we obtain a linear system of equations that we need to solve

$$\mathbf{A}\mathbf{d} = \mathbf{s}\,. \tag{17}$$

This routine has already been implemented in Alba Muixí's code, so we are not going to perform any testing on it.

3.3 Algorithm

Once reviewed the two equations that constitute (3) we state the general algorithm that we will follow to solve our problem.

For $n = 1, 2, \dots, nOfSteps$:

1. Compute $\ddot{\mathbf{U}}^{n+1}$ solving (12).
2. Compute $\mathbf{U}^{n+1}$ and $\dot{\mathbf{U}}^{n+1}$ using (10).
3. Set the Dirichlet nodal values in $\mathbf{U}^{n+1}$.
4. Update $\mathcal{H}(\mathbf{u})$ at the nodes.
5. Compute d^{n+1} solving (17).
6. Update the partition Ω_1, Ω_2 and Γ, identifying new elements to be refined, i.e., elements with $\max(d_i^e) \geq 0.2$.

end

Note that the boundary conditions for the equilibrium equation are imposed after the computation of step 2.

4. L-shaped test

We consider an L-shaped piece attached at the bottom. That is, we impose 0 displacement at the nodes on the bottom boundary ($u = 0$). We then impose an upward vertical displacement $u_y = u_D(t)$ on the node placed at $(220, 0)$, as shown in Figure 7. This displacement will depend quadratically on time during the first seconds of the experiment, and then it will proceed with a constant velocity until the end of the simulation. More precisely, we impose

$$u_D(t) = \begin{cases} \frac{1}{2} \cdot 10^{-2} t^2 & t \leq 0.1\,, \\ 10^{-3} t - 5 \cdot 10^{-5} & t \geq 0.1\,, \end{cases} \tag{18}$$

for the equilibrium equation and homogeneous Neumann boundary conditions for the damage equation.

As a result of the imposed displacement, the piece will undergo a deformation that will lead to a crack propagated along the piece. As it can be seen in the picture, we consider a uniform mesh of quadrilateral linear elements. We will refine the three elements that are on the corner of the piece, so that we can capture the crack initiation. As the experiment progresses and the crack evolves, more elements will be refined in order to capture the whole solution.

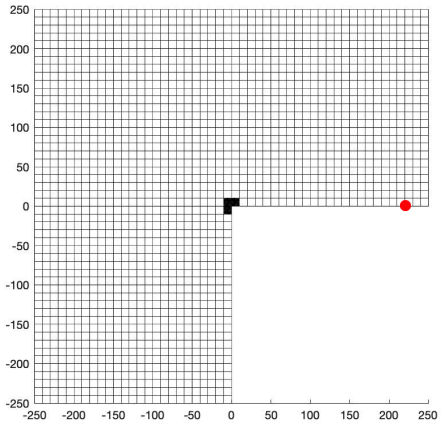

Figure 7: Discretization of an L-shaped piece using a uniform mesh of quadrilateral linear elements. The refinement on the corner of the piece can be observed.

In this simulation we consider $E = 25.8423\,GPa$, $\nu = 0.18$, $\rho = 2.35 \cdot 10^{-9}\,kg/mm^3$, $G_c = 8.9 \cdot 10^{-5}\,kN/mm^2$ and $l = 3\,mm$. For the refinement of the elements, we choose a factor of $m = 15$. As initial conditions, we will take $\mathbf{u}^0 = 0$, $\dot{\mathbf{u}}^0 = 0$ and $d^0 = 0$.

The system has been integrated up to $t = 400\,s$ and we have used 3 different time steps: $\Delta t = 0.4$, $\Delta t = 0.04$ and $\Delta t = 0.004$. In Figure 8 we can see the evolution of the crack taking $\Delta t = 0.004$.

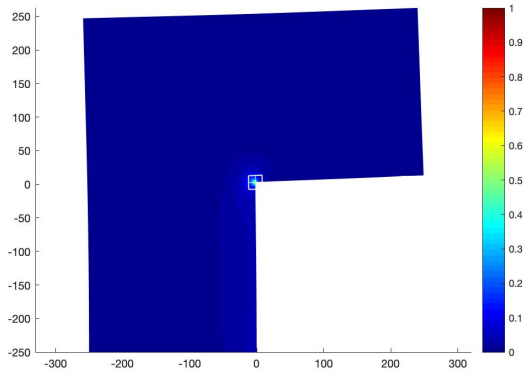

(a) $t = 250\,s$.

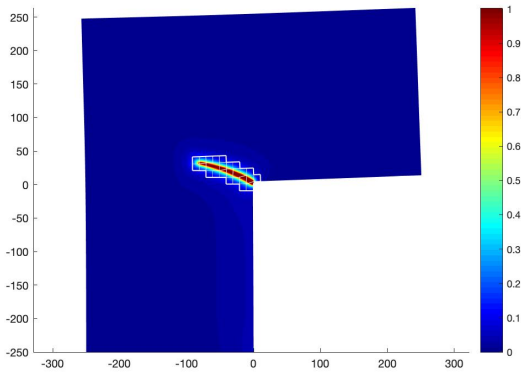

(b) $t = 260\,s$.

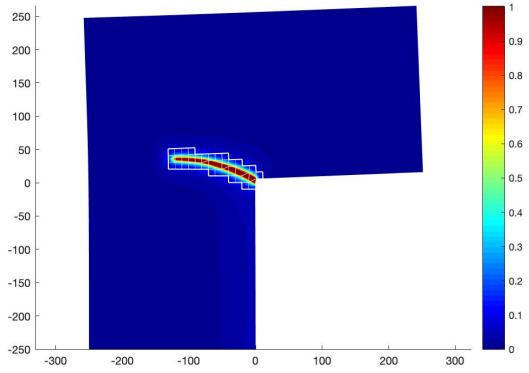

(c) $t = 300\,s$.

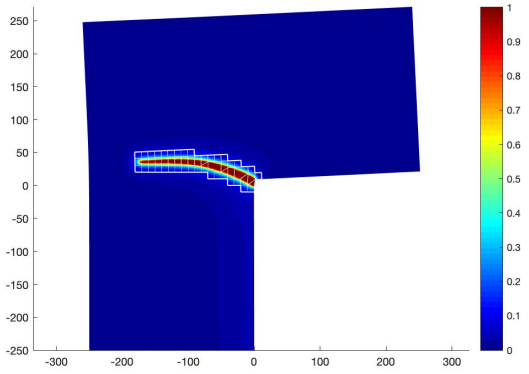

(d) $t = 400\,s$.

Figure 8: Damage variable d showing the evolution of the crack along time. Displacements are amplified by a factor of 50.

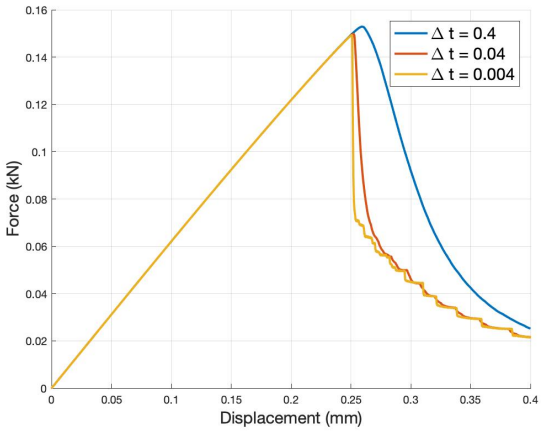

Figure 9: Force-Displacement graphic for different values of Δt.

In Figure 9 we show the force-displacement plots for different values of Δt. The plots depict the force that we would need to apply to the piece in order to reach the imposed displacement u_D, that is the reaction force. As it can be seen in the plot, all three curves start as straight lines until they reach an approximate displacement of 0.26 mm, the point where the piece breaks and the crack emerges. From then on, the force needed to continue displacing the piece is smaller, since the crack makes it easier to move. We can also see that, the smaller the time step Δt is, the more similar the curves are, showing convergence in time.

Once we have seen the first simulation with the aforementioned parameters, we what are going to do now is to repeat it changing the values of some of those variables, in order to better understand their effect on the result. $\Delta t = 0.04$ is considered in the following experiments to study the outcome of G_c, l and the load velocity $\dot{u}_D$.

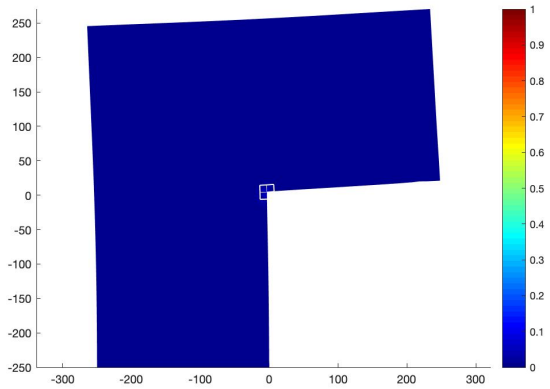

(a) $G_c = 8.9 \cdot 10^{-4}\, kN/mm^2$.

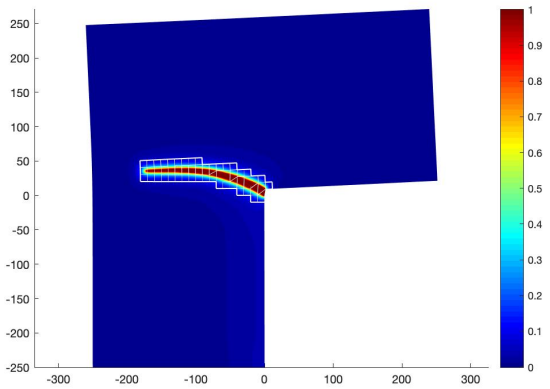

(b) $G_c = 8.9 \cdot 10^{-5}\, kN/mm^2$.

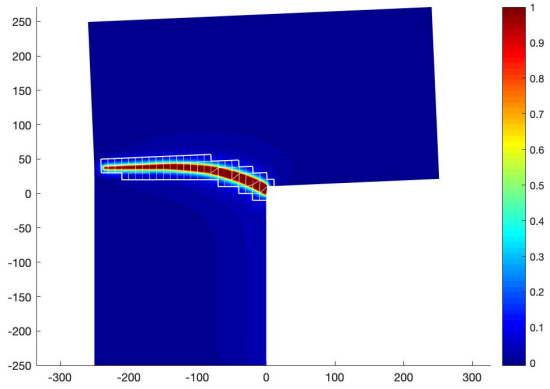

(c) $G_c = 8.9 \cdot 10^{-6}\, kN/mm^2$.

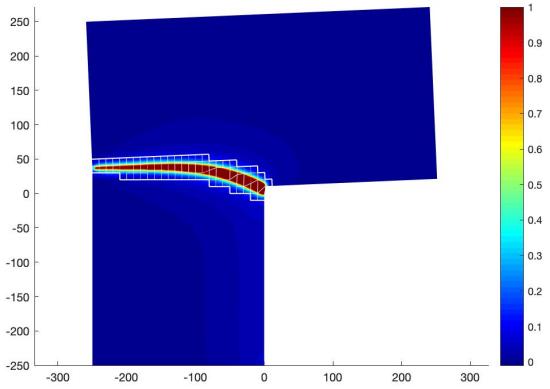

(d) $G_c = 8.9 \cdot 10^{-7}\, kN/mm^2$.

Figure 10: Cracks at time $t = 400\, s$ generated varying G_c and keeping the other parameters.

As it can be seen in Figure 10, the variable G_c controls the "speed" of the crack, as it is the critical energy release rate, a value that, when reached, allows the crack to grow. The larger G_c is, the longer it takes to break and, thus, the result looks less damaged. On the contrary, the smaller it is, the faster the piece breaks.

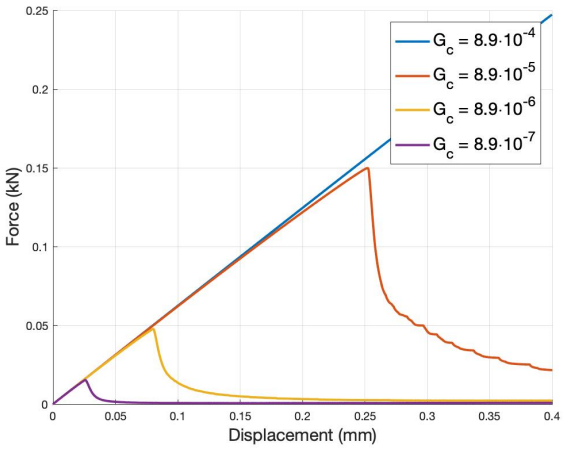

Figure 11: Force-Displacement plots for different values of G_c.

In this case we have also plotted the force-displacement graphic (see Figure 11). As it can be seen in the plot, for $G_c = 8.9 \cdot 10^{-4}\, kN/mm^2$ we see just a straight line, since the piece has not broken and, thus, the force needed to produce the displacement never decreases. We can see how the break happens earlier as we decrease the value of G_c.

The next variable we study is l. As it can be seen in Figure 12, l controls the width of the smoothed crack. This is due to the fact that this parameter appears multiplying the diffusion coefficient in the damage equation, that is, if we increase l, we increase the diffusion and, thus, the width of the crack. It is important to note that very large values of this variable can lead to results that make no physical sense. In order to properly represent brittle fracture we need l as small as we can, that is $l \longrightarrow 0$. We need to take into account, however, that if we decrease the value of l we need to increase the refinement factor m, in order to fully capture the crack's path. We can choose this parameter by using

$$m = \left\lceil \frac{4h}{lp} \right\rceil, \tag{19}$$

where p is the degree of the approximation and h is the size of the elements on the coarse mesh (standard elements).

In order to get a better understanding of the results, we have plotted the force-displacement graphic for the same values of l. As we can see in Figure 13, the curves follow a linear behaviour until they reach $0.25\, mm$, approximately, the point where the break is produced and so the curves start to decrease. We can see how for the smallest value of the parameter l the curve oscillates a bit after the crack is produced. This is probably due to the fact that the value of l is very small and we should use a smaller time step Δt in order to capture the crack with more accuracy.

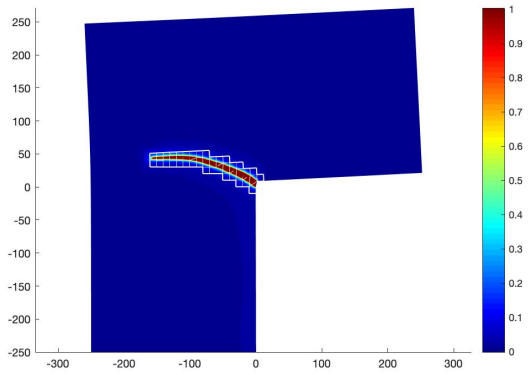

(a) $l = 1.5\,mm$.

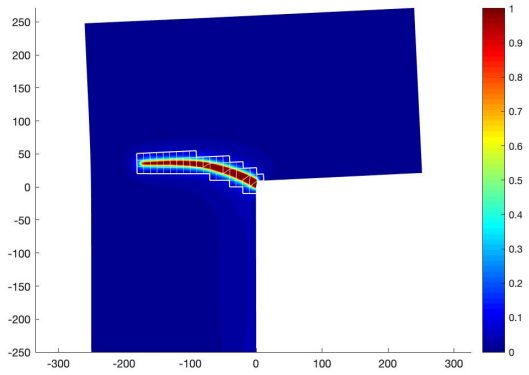

(b) $l = 3\,mm$.

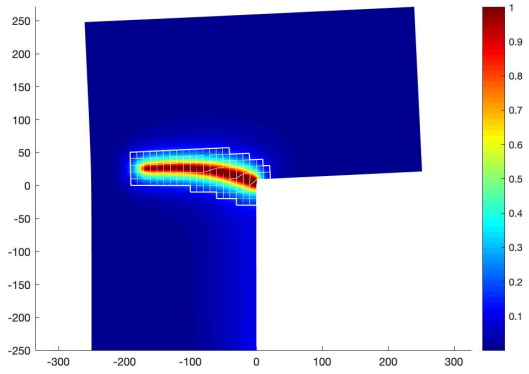

(c) $l = 10\,mm$.

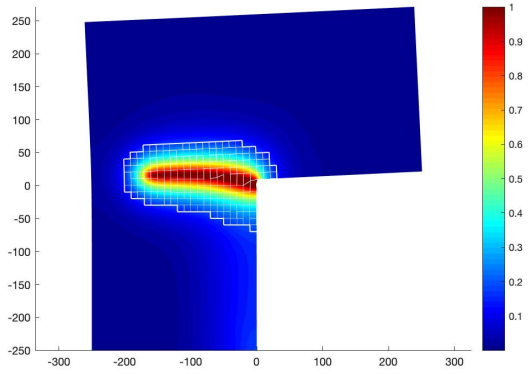

(d) $l = 20\,mm$.

Figure 12: Cracks at $t = 400\,s$ generated varying l and keeping the other parameters.

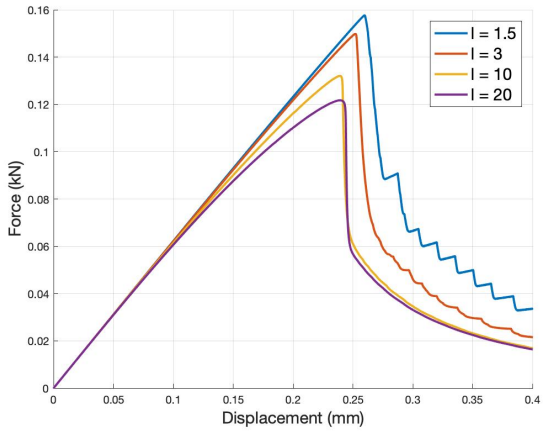

Figure 13: Force-Displacement plots for different values of l.

To finish with the study of the variables we consider the load velocity. In particular, we take

$$u_D^1(t) = \begin{cases} 5 \cdot 10^{-2} t^2 + 4.5 \cdot 10^{-4} & t \leq 0.1\,, \\ 10^{-2} t - 5 \cdot 10^{-5} & t \geq 0.1\,, \end{cases} \qquad u_D^2(t) = \begin{cases} 25 \cdot 10^{-3} t^2 + 2 \cdot 10^{-4} & t \leq 0.1\,, \\ 5 \cdot 10^{-3} t - 5 \cdot 10^{-5} & t \geq 0.1\,, \end{cases}$$

$$u_D^3(t) = \begin{cases} \frac{1}{2} \cdot 10^{-2} t^2 & t \leq 0.1\,, \\ 10^{-3} t - 5 \cdot 10^{-5} & t \geq 0.1\,, \end{cases} \qquad u_D^4(t) = \begin{cases} 25 \cdot 10^{-4} t^2 + 7.5 \cdot 10^{-5} & t \leq 0.1\,, \\ 5 \cdot 10^{-4} t + 5 \cdot 10^{-5} & t \geq 0.1\,, \end{cases}$$

that is, $\dot{u}_D^1(t) = 10^{-2}$, $\dot{u}_D^2(t) = 5 \cdot 10^{-3}$, $\dot{u}_D^3(t) = 10^{-3}$ and $\dot{u}_D^4(t) = 5 \cdot 10^{-4}$, for $t \geq 0.1$.

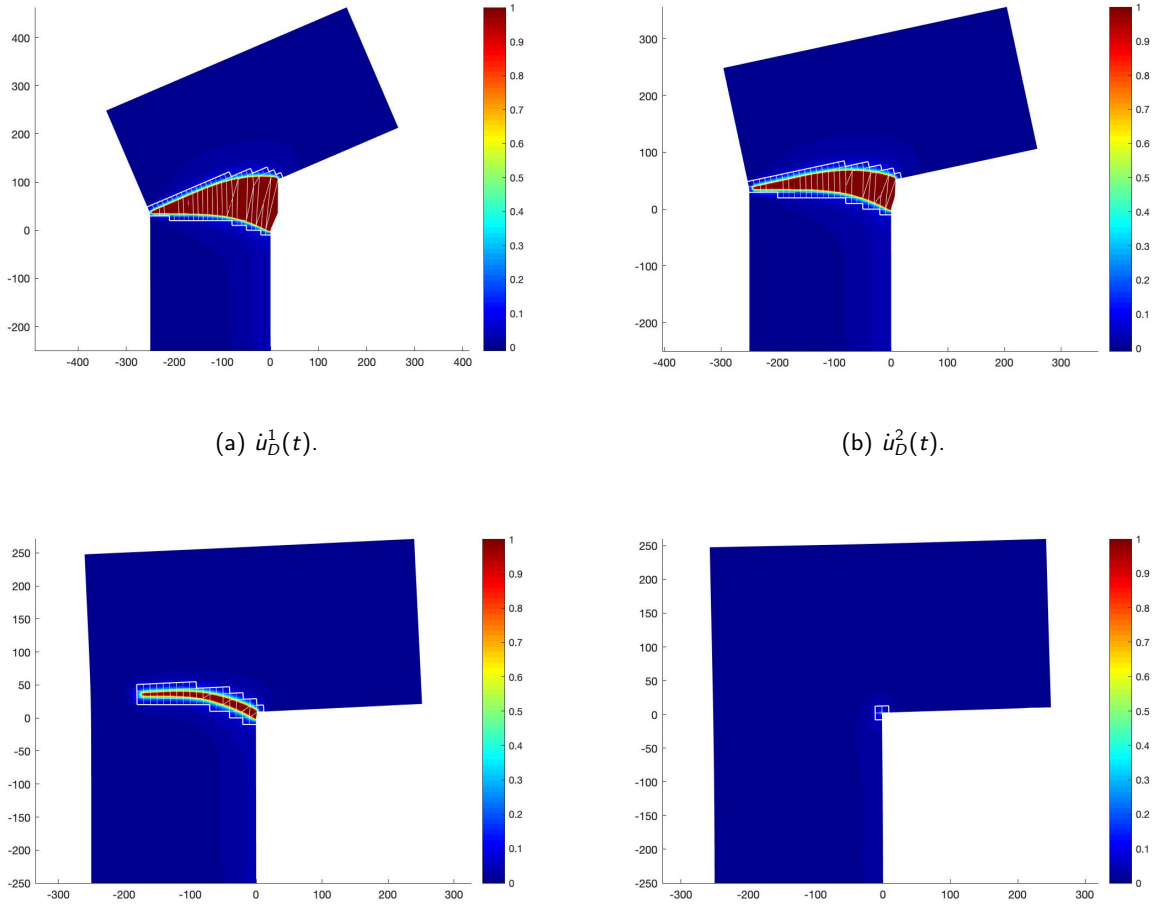

(a) $\dot{u}_D^1(t)$. (b) $\dot{u}_D^2(t)$.

(c) $\dot{u}_D^3(t)$. (d) $\dot{u}_D^4(t)$.

Figure 14: Cracks at time $t = 400\,s$ generated varying $\dot{u}_D(t)$ and keeping the other parameters.

As it can be seen in Figure 14, the larger $\dot{u}_D(t)$ is, the more and the faster the piece breaks. Let us also note that for very small values of $\dot{u}_D(t)$ (as, for example, the last case), the piece does not have enough time to break. We can also see that increasing the load velocity $\dot{u}_D(t)$ does not affect the path the crack takes. Note also that in all cases we have integrated the system up to $t = 400\,s$.

As we did with the other variables, we have also plotted the force-displacement graphic, that can be seen in Figure 15. We can see how for $\dot{u}_D^4(t)$ the piece has not broken, as the curve is a straight line. For the other cases, we can see how the piece breaks more or less at the same point but, since we have changed the displacements $u_D(t)$, the final displacement is bigger in some cases.

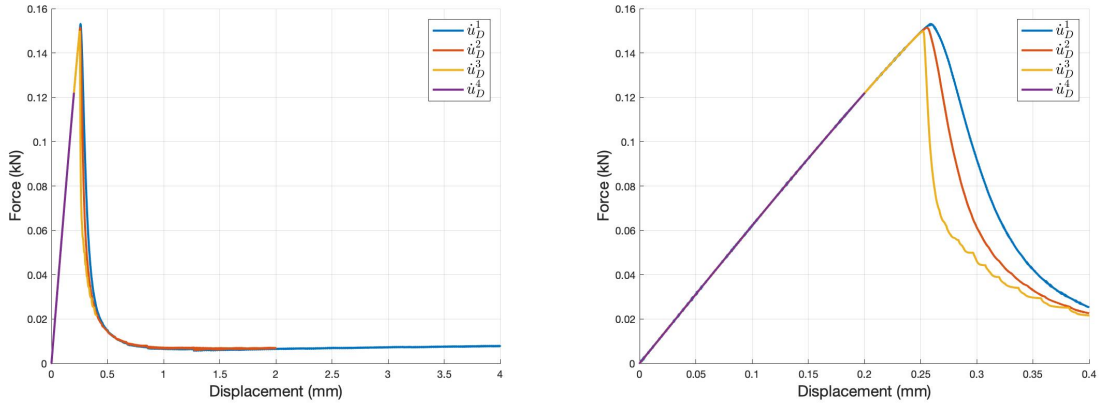

(a) Whole plots.

(b) Zoom of the plots.

Figure 15: Force-Displacement plots for different values of $\dot{u}_D(t)$.

5. Branching test

We aim now to test the phase-field model with some branching. This phenomenon is produced when the material is under great stress and it cannot dissipate all the energy in a single crack. In order to do this testing we will take the specifications of the piece and the parameters from the branching example on [9].

We consider a rectangular piece of size $100 \times 40\, mm$, to which we apply a constant tension of $\sigma = 10^{-3}\, GPa$ on the top and the bottom during the whole simulation. The piece has an initial horizontal crack from the left to the centre with a width of $l = 1.25\, mm$ that we model with the initial condition $d^0 = 1$.

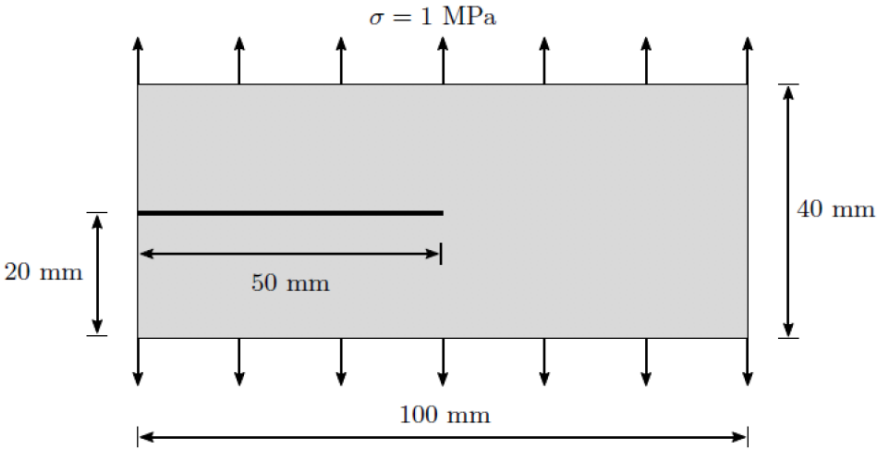

Figure 16: Piece size and boundary conditions of the problem. Figure from [9].

As we did with the L-shaped example, in order to solve the problem we consider a uniform mesh of quadrilateral linear elements. In this case will refine the elements surrounding the initial crack, that is the ones satisfying $x \leq 0\, \& \, -l/2 \leq y \leq l/2$. As before, as the experiment progresses and the crack evolves, more elements will be refined in order to capture the whole solution.

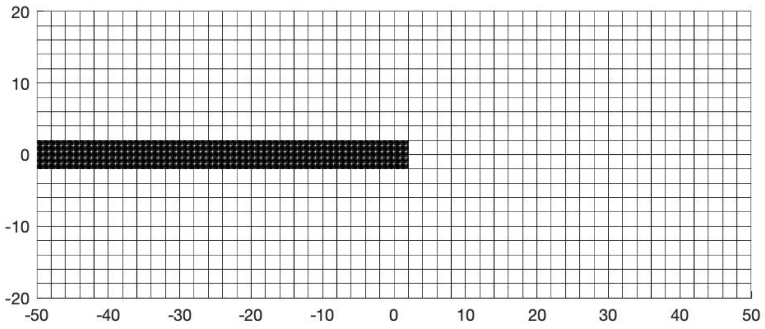

Figure 17: Discretization of the piece using a uniform mesh of quadrilateral linear elements. The refinement of the initial crack can be observed.

In this simulation we consider $E = 32\,GPa$, $\nu = 0.2$, $G_c = 6 \cdot 10^{-6}\,kN/mm^2$, $\rho = 2.45 \cdot 10^{-9}\,kg/mm^3$ and $l = 1.25\,mm$. As the other example, for the refinement of the elements we are going to choose a factor of $m = 15$. As initial conditions for the displacements we will take $\mathbf{u}^0 = 0$, $\dot{\mathbf{u}}^0 = 0$ and for the damage will consider $d^0 = 0$ in the whole domain, except for the initial crack, where we impose $d^0 = 1$. This initial crack is modelled as a Dirichlet condition for the damage equation: we will impose $d = 1$ to all nodes within the previous described domain: $x \leq 0\,\&\, -l/2 \leq y \leq l/2$. The tensions to which the piece is subject to are imposed using Neumann conditions for the equilibrium equation. That is, we will impose

$$\sigma \cdot \mathbf{n} = \mathbf{t}_N = \begin{bmatrix} 0 \\ \pm 10^{-3} \end{bmatrix}.$$

We will integrate the system up to $t = 0.004\,s$ with three different time steps: $\Delta t = 8 \cdot 10^{-6}$, $\Delta t = 4 \cdot 10^{-6}$ and $\Delta t = 8 \cdot 10^{-7}$. In Figure 18 we can see the solution for $\Delta t = 8 \cdot 10^{-7}$ at different moments of the simulation. We can see how at the beginning the initial crack is just propagated forward but at a certain point it branches into two cracks until the end of the simulation.

For this testing we are also going to study the energies that play a significant role in the problem, a computation that is often made in this kind of simulations. We will consider the elastic energy, the one stored by the material due to the fact that the piece is under deformation, and the fracture energy, the one discharged by the material because of the crack.

$$E_{elas} = \int_\Omega (1-d)^2 \varepsilon : \mathcal{C} : \varepsilon \, d\Omega\,, \qquad E_{frac} = G_c \int_\Omega \left(\frac{d^2}{2l} + \frac{l}{2} |\nabla d|^2 \right) d\,\Omega\,. \tag{20}$$

Although we could use (20) to compute the energies, in practice the matrices of the systems are used to do the computations, since it is way cheaper, computationally speaking. Thus,

$$E_{elas} = \frac{1}{2} \mathbf{u}^T \mathbf{K}^{eq} \mathbf{u}\,, \qquad E_{frac} = d^T \mathbf{A} d\,, \tag{21}$$

where $\mathbf{u}$ is the nodal vector of displacements, $\mathbf{K}^{eq}$ is the stiffness matrix for the equilibrium problem, d is the nodal vector of damage and $\mathbf{A}$ is computed by means of a geometrical mass matrix $\mathbf{M}$ and a diffusivity matrix $\mathbf{D}$:

$$\mathbf{A} = \frac{G_c}{2l}\mathbf{M} + \frac{G_c l}{2}\mathbf{D}\,, \qquad \text{with} \quad \mathbf{M} = \int_\Omega N_i N_j \, d\Omega\,, \quad \mathbf{D} = \int_\Omega \nabla N_i \nabla N_j \, d\Omega\,.$$

In Figure 19 both energies are displayed for each of the time steps Δt. We can see that fracture energy increases as the simulation advances and it becomes constant at the end, when the piece is completely broken. The elastic energy, however, has different peaks, that correspond to an advance of the crack. It is also important to note that this energy keeps increasing until we reach $t = 0.002\,s$, moment where the branching is produced and the elastic energy tends to decrease.

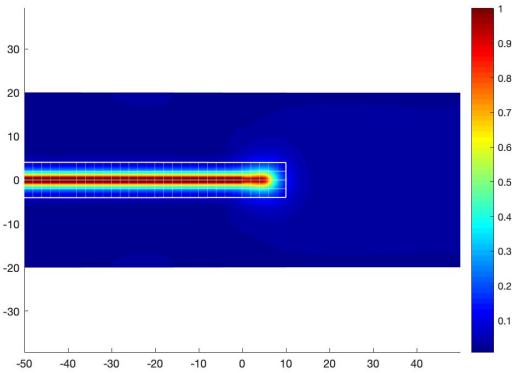

(a) $t = 0.001\,s$.

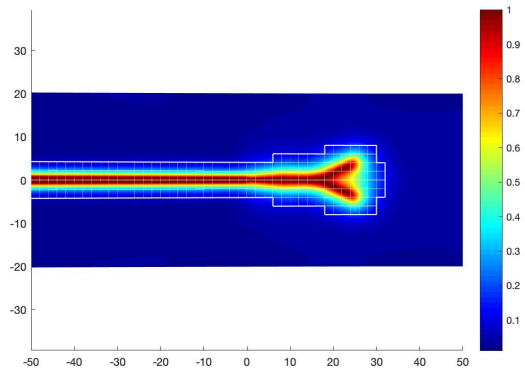

(b) $t = 0.002\,s$.

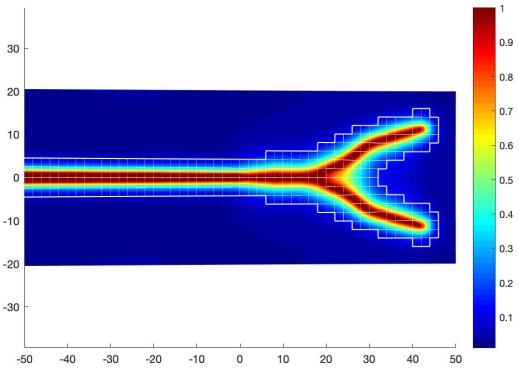

(c) $t = 0.003\,s$.

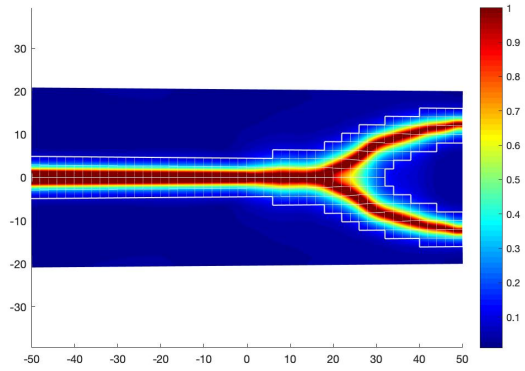

(d) $t = 0.004\,s$.

Figure 18: Damage variable d showing the evolution of the crack along time. Displacements have been amplified by 5.

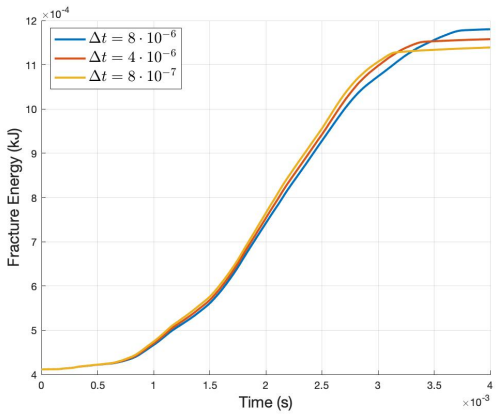

(a) Fracture energy.

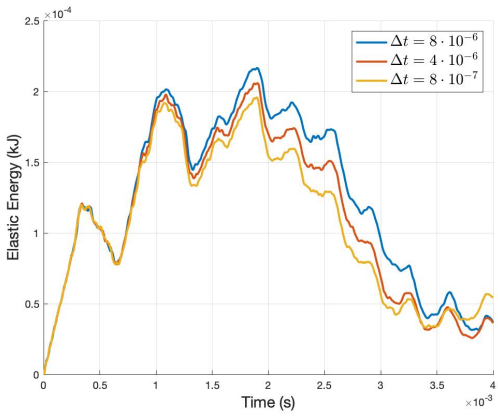

(b) Elastic energy.

Figure 19: Evolution of the fracture and elastic energies throughout time.

Once seen the simulation with the aforementioned parameters has been seen, we are going to repeat it changing the values of some of those variables, in order to better understand their effect on the result. We will the outcome of G_c, l and the applied stress $\mathbf{t}_N$.

The first parameter we test is the critical energy release rate G_c, that controls how easy to fracture the material is. As it can be seen in Figure 20, this resistance is also translated into different shapes of the branches. We can also see that the larger the value of G_c is, the earlier the branching is produced. This can be explained if we think that when G_c is large the material accumulates a lot of energy, that cannot be dissipated through a unique branch, so it needs to bifurcate earlier.

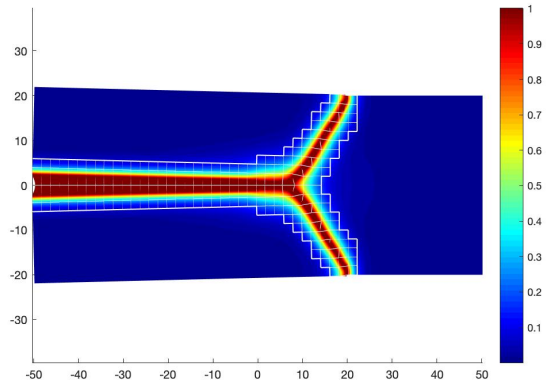

(a) $G_c = 1 \cdot 10^{-4}$.

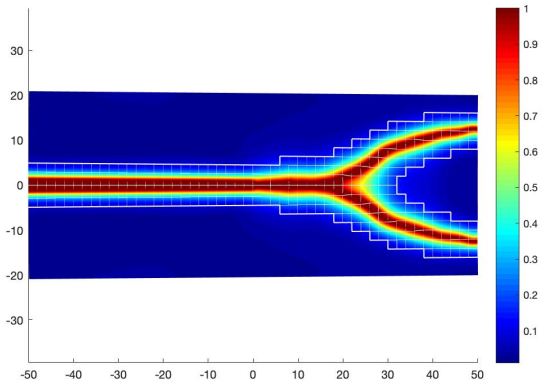

(b) $G_c = 6 \cdot 10^{-6}$.

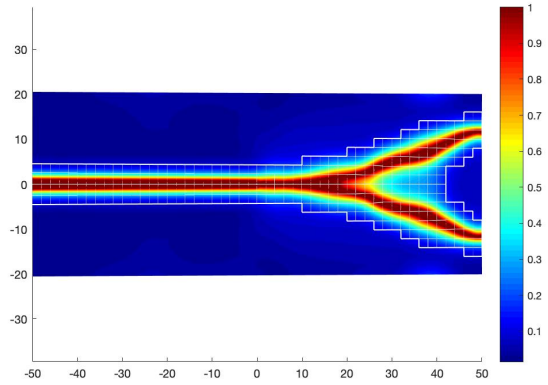

(c) $G_c = 3 \cdot 10^{-6}$.

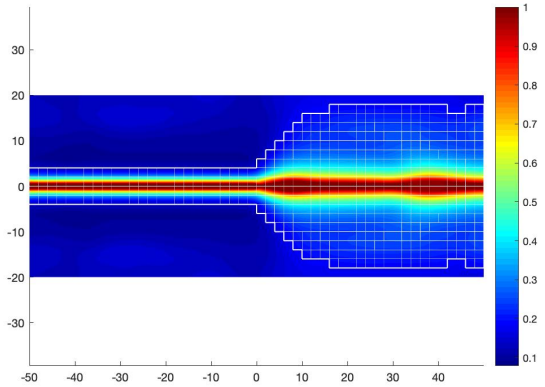

(d) $G_c = 5 \cdot 10^{-7}$.

Figure 20: Cracks generated varying G_c and keeping the other variables.

In Figure 21a we can see that the larger the value of G_c is, the more time the cracks need to advance, due to the own definition of the constant. Let us note that, in this particular case, we have integrated the system up to different times, since we wanted to make clear the condition of the variable. The elastic energy seen in Figure 21b reaches a higher peak the larger G_c is.

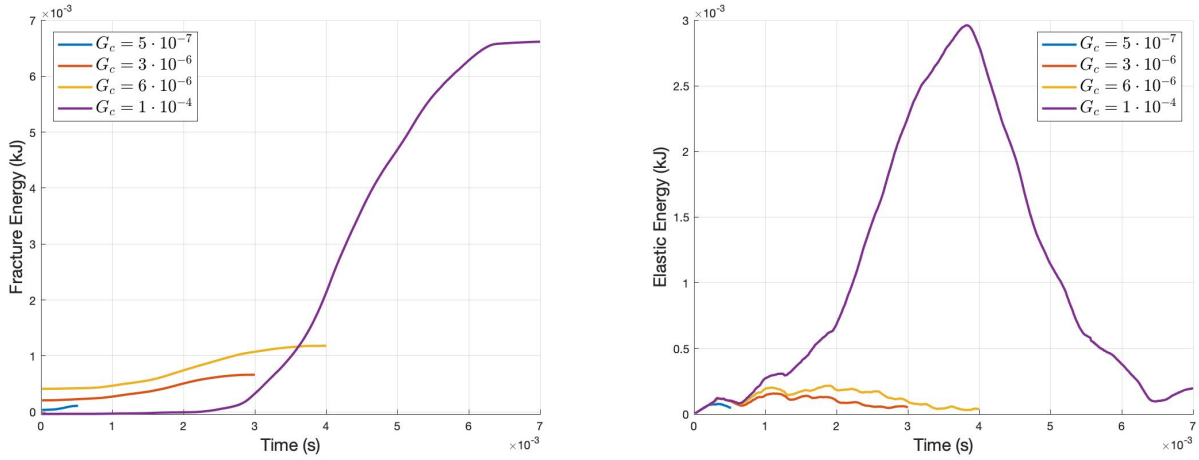

(a) Fracture energy.

(b) Elastic energy.

Figure 21: Evolution of the fracture and elastic energies throughout time.

We will continue by analysing the variable l. As it can be seen in Figure 22, this variable controls the width of the crack. The larger l is, the wider the crack becomes. As we did with the L-shaped case, we need to take into account that if we decrease the value of l we need to increase the refinement factor m, in order to fully capture the crack's path. That is why we are going to use chose m based on (19).

As in the other cases, we have plotted the fracture and elastic energies for the different values of l. In Figure 23 we can see how the fracture energy has the expected behaviour, increasing as the crack advances and becoming constant when the piece has completely broken. The elastic energy is also as expected, increasing at the beginning and decreasing when the branch is produced.

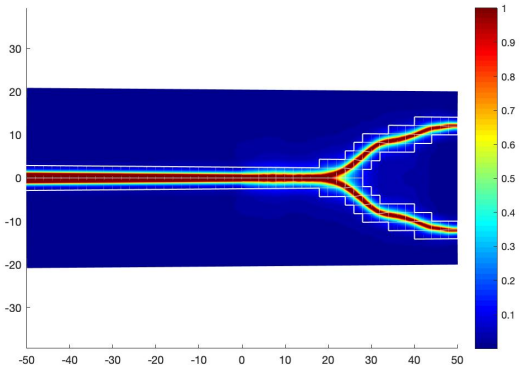

(a) $l = 0.5\,mm$.

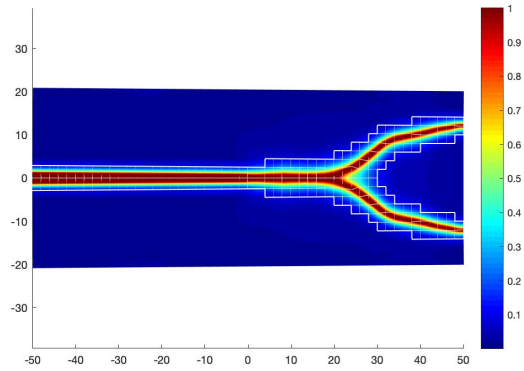

(b) $l = 0.75\,mm$.

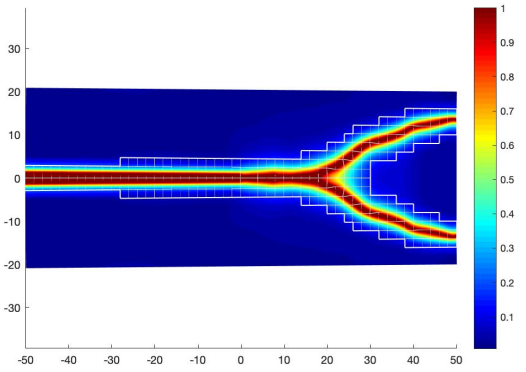

(c) $l = 1\,mm$.

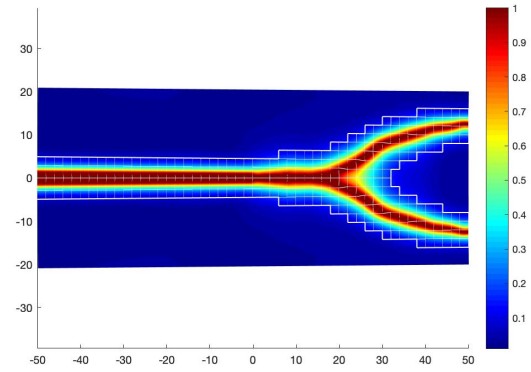

(d) $l = 1.25\,mm$.

Figure 22: Cracks generated varying l and keeping the other parameters.

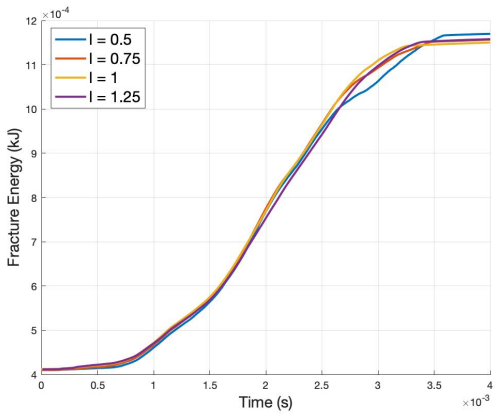

(a) Fracture energy.

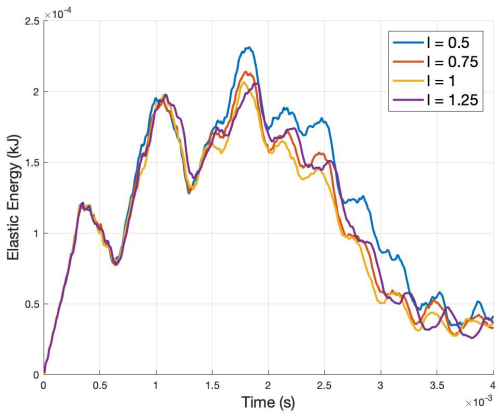

(b) Elastic energy.

Figure 23: Evolution of the fracture and elastic energies throughout time.

To finish the study, we analyse the applied stress. That is, we will vary the value of t_N^2 in

$$\sigma \cdot \mathbf{n} = \mathbf{t}_N = \begin{bmatrix} 0 \\ \pm t_N^2 \end{bmatrix}.$$

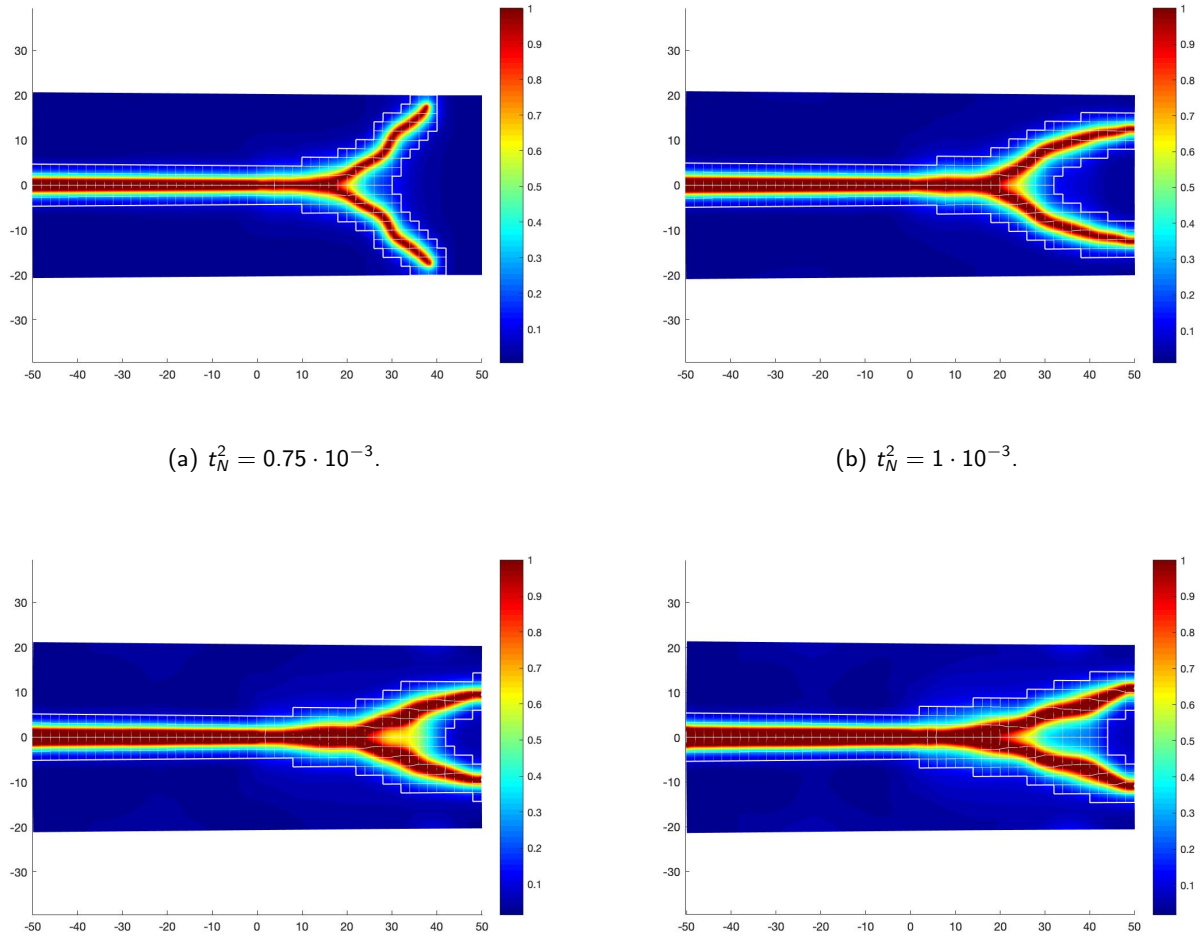

(a) $t_N^2 = 0.75 \cdot 10^{-3}$.

(b) $t_N^2 = 1 \cdot 10^{-3}$.

(c) $t_N^2 = 1.25 \cdot 10^{-3}$.

(d) $t_N^2 = 1.5 \cdot 10^{-3}$.

Figure 24: Cracks generated varying t_N^2 and keeping the other parameters.

The bigger t_N^2 is, the stronger the applied stress is and, as it can be seen in Figure 24, the more damage is produced on the piece. We can also see that as we increase the value of t_N^2 the branching is produced a little later and the branches are closer between them.

The energies plotted in Figure 25 depict what we have already seen: the fracture energy increases as the simulation advances, becoming constant in the cases where the piece gets completely broken, while the elastic energy keeps oscillating as the crack advances. Note that for $t_N^2 = 1.5 \cdot 10^{-3}$ the elastic energy increases at the end, probably because of the massive damage the piece is subjected to.

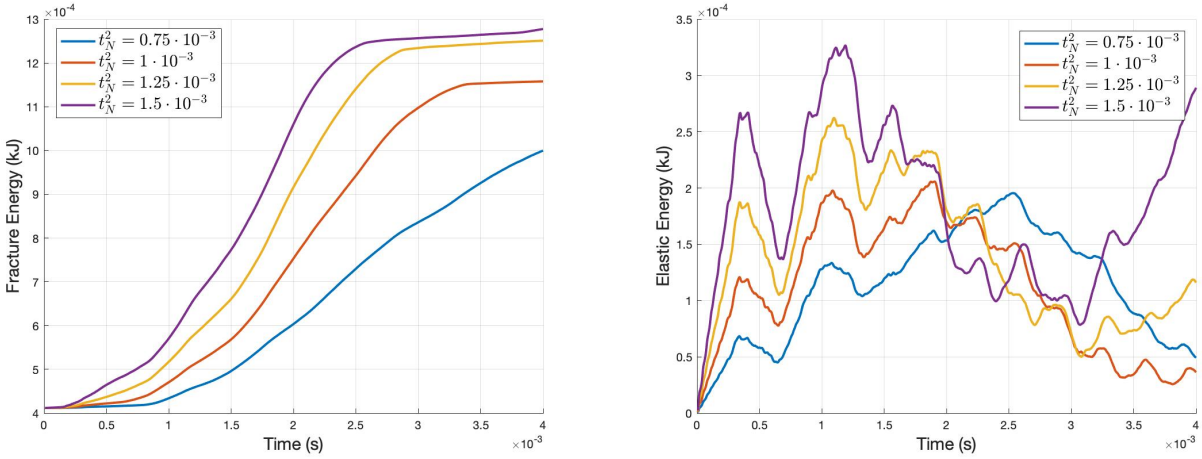

(a) Fracture energy.

(b) Elastic energy.

Figure 25: Evolution of the fracture and elastic energies throughout time.

6. Conclusions

The main objective of this project was to adapt the refinement strategy developed in [6] to work with a dynamic phase-field model, so we do not have to do a manual adaptation of the mesh, as the author of [2] had to do. Once the phase-field model has been derived, we have defined some tools needed for the adaptive refinement, such as the notion of a broken domain $\Omega = \Omega_1 \cup \Omega_2$. Then, we have stated the weak forms of the equilibrium and the damage equations using Nitsche's method (to impose continuity in weak form between the refined and the standard domains, i.e., at $\Omega_1 \cap \Omega_2$) and we have used the so-called Newmark's method in order to solve, in an implicit way, the linear system of ODEs obtained after discretizing the equilibrium equation's weak form.

The procedure has been tested with two different examples. The first one was an L-shaped piece attached at the bottom and subjected to an upward vertical displacement imposed at one node in order to produce a crack. We also studied the parameters that take action in the simulation: G_c, l and the load velocity $\dot{u}_D$. To do so, besides computing the solution we have also plotted the force-displacement graphic to help us better understand the behaviour of the solution when a variable is changed.

The other example was a rectangular piece with a constant stress applied on the top and the bottom during the whole simulation. As we did with the first example we also studied the parameters involved: G_c, l and the applied stress $\mathbf{t}_N$. The results of the simulation are coupled with energy plots, that describe the energy stored by the material due to the fact that the piece is under deformation (elastic energy), and the energy discharged by the material because of the crack (fracture energy).

The elaboration of this project has given me an opportunity to use my basic knowledge of the Finite Element method on a more sophisticated problem. Although I had previously worked on the phase-field model, the introduction of the temporary variable and the use of two different types of elements, standard and refined, have been a major challenge. The fact that most of the simulation took a few days, although using the LaCan's cluster *Clonetroop*, was also a hurdle, since I had to make sure everything was OK before starting the computations, as a tiny mistake could delay the whole project for days.

During the development of the work we became interested in further studies, that are currently in development. Newmark's method is an implicit method, that is unconditionally stable although it is somewhat slow since it has to solve a linear system of equations at each time step, so a natural step to take was to try to solve the system of ODEs using an explicit method. We tried to use a centred differences approximation, although the method did not converge even with very small time steps Δt. We guess that the reason is that this time integration scheme may not be suited for this kind of Differential Algebraic Equation (DAE). That is why a future work could be doing some research on other explicit methods that could work, or even a slight variation of the phase-field model that could give more stability and allow an explicit method as a solver. One option could be, for example, adding a damage velocity on the damage equation as in [3].

References

[1] Bourdin, B., Francfort, G.A., Marigo, J.J.. (2008). *The variational approach to fracture.* Journal of Elasticity 91, p. 5 - 148. https://doi.org/10.1007/s10659-007-9107-3.

[2] de la Torre, S.. (2019). *Model de Phase-Field dinàmic per a fractura fràgil.* Degree thesis. https://upcommons.upc.edu/bitstream/handle/2117/166625/memoria.pdf.

[3] Hofacker, M & Miehe, C.. (2013). *A phase field model of dynamic fracture: Robust field updates for the analysis of complex crack patterns.* International Journal for Numerical Methods in Engineering 93, p. 276 - 301. https://doi.org/10.1002/nme.4387.

[4] Miehe, C., Hofacker, M., Welschinger, F.. (2010). *A phase-field model for rate-independent crack propagation: Robust algorithmic implementation based on operator splits.* Computer Methods in Applied Mechanics and Engineering 199.45-48, p. 2765 - 2778. https://doi.org/10.1016/j.cma.2010.04.011.

[5] Muixí, A. (2018) *An HDG phase-field model with transition to fracture for crack propagation.* PhD in Applied Mathematics - Research plan.

[6] Muixí, A., Fernández-Méndez, S. & Rodríguez-Ferran, A.. (2020). *Adaptive refinement for phase-field models of brittle fracture based on Nitsche's method.* Comput Mech 66, p. 69 - 85. https://doi.org/10.1007/s00466-020-01841-1

[7] Muxí, A., Fernández-Méndez, S. & Rodríguez-Ferran, A.. (2018). *A hybridizable discontinuous Galerkin phase-field model for brittle fracture.* Reports @SCM 4.1, p. 31 - 42. https://doi.org/10.1002/nme.6260.

[8] Pons, A.. (2019). *Models computacionals de fractura fràgil.* Degree thesis. https://upcommons.upc.edu/bitstream/handle/2117/127306/memoria.pdf.

[9] Rudy JM Geelen et al.. (2019). *A phase-field formulation for dynamic cohesive fracture.* 348, p. 680 - 711. https://doi.org/10.1016/j.cma.2019.01.026

A. Weak form of the Equilibrium equation

In this appendix we will deduce the weak form for the equilibrium equation

$$\begin{cases} \rho\ddot{\mathbf{u}} = \nabla \cdot \boldsymbol{\sigma} & \text{in } \Omega\,, \\ \boldsymbol{\sigma} = (1-d)^2\mathcal{C} : \varepsilon(\mathbf{u}) & \\ \mathbf{u} = \mathbf{u}_D & \text{on } \Gamma_D\,, \\ \boldsymbol{\sigma}(\mathbf{u}) \cdot \mathbf{n} = \mathbf{t}_N & \text{on } \Gamma_N\,. \end{cases} \tag{22}$$

To obtain its weak form, we multiply the first equation of (22) by a function $\mathbf{v}$ such that $\mathbf{v} = 0$ on Γ_D, and then integrate on both sides of the equation:

$$\int_\Omega \rho\mathbf{v} \cdot \ddot{\mathbf{u}}\; d\Omega = \int_\Omega \mathbf{v} \cdot (\nabla \cdot \boldsymbol{\sigma})\; d\Omega\,. \tag{23}$$

Using now

$$\nabla \cdot (\mathbf{v} \cdot \boldsymbol{\sigma}) = \nabla\mathbf{v} : \boldsymbol{\sigma} + \mathbf{v} \cdot (\nabla \cdot \boldsymbol{\sigma})\,,$$

on (23), we get

$$\int_\Omega \rho\mathbf{v} \cdot \ddot{\mathbf{u}}\; d\Omega + \int_\Omega \nabla\mathbf{v} : \boldsymbol{\sigma}\; d\Omega = \int_\Omega \nabla \cdot (\mathbf{v} \cdot \boldsymbol{\sigma})\; d\Omega\,.$$

Applying now the divergence theorem, we obtain

$$\int_\Omega \rho\mathbf{v} \cdot \ddot{\mathbf{u}}\; d\Omega + \int_\Omega \nabla\mathbf{v} : \boldsymbol{\sigma}\; d\Omega = \int_{\partial\Omega} \mathbf{v} \cdot \boldsymbol{\sigma} \cdot \mathbf{n}\; d\partial\Omega\,,$$

where $\mathbf{n}$ is the exterior normal vector. Splitting now $\partial\Omega = \Gamma_N \cup \Gamma_D \cup \Gamma$, where Γ is the Nitsche's boundary, we get

$$\int_\Omega \rho\mathbf{v} \cdot \ddot{\mathbf{u}}\; d\Omega + \int_\Omega \nabla\mathbf{v} : \boldsymbol{\sigma}\; d\Omega = \int_{\Gamma_D} \mathbf{v} \cdot \boldsymbol{\sigma} \cdot \mathbf{n}\; d\Gamma_D + \int_{\Gamma_N} \mathbf{v} \cdot \boldsymbol{\sigma} \cdot \mathbf{n}\; d\Gamma_N + \int_\Gamma \mathbf{v} \cdot \boldsymbol{\sigma} \cdot \mathbf{n}\; d\Gamma\,.$$

Since we have chosen $\mathbf{v}$ such that $\mathbf{v} = 0$ on Γ_D and, by (22), we have that $\boldsymbol{\sigma}(\mathbf{u}) \cdot \mathbf{n} = \mathbf{t}_N$ on Γ_N, we get to the weak form of the problem:

$$\int_\Omega \rho\mathbf{v} \cdot \ddot{\mathbf{u}}\; d\Omega + \int_\Omega \nabla\mathbf{v} : \boldsymbol{\sigma}\; d\Omega = \int_{\Gamma_N} \mathbf{v} \cdot \mathbf{t}_N\; d\Gamma_N + \int_\Gamma \mathbf{v} \cdot \boldsymbol{\sigma} \cdot \mathbf{n}\; d\Gamma\,.$$

B. Weak form of the damage equation

In this appendix we will deduce the weak form for the damage equation

$$\begin{cases} -l^2\Delta d + d = \dfrac{2l}{G_c}(1-d)\mathcal{H} & \text{in } \Omega\,, \\ \nabla d \cdot \mathbf{n} = 0 & \text{on } \Gamma_N\,. \end{cases} \tag{24}$$

For the sake of helping the calculation, we rearrange it as

$$\begin{cases} \left(\dfrac{G_c}{l} + 2\mathcal{H}\right) d - G_c l \Delta d = 2\mathcal{H} & \text{in } \Omega\,, \\ \nabla d \cdot \mathbf{n} = 0 & \text{on } \Gamma_N\,. \end{cases} \tag{25}$$

To obtain its weak form, we multiply the first equation of (25) by a function v and then integrate on both sides of the equation:

$$\int_\Omega \left(\frac{G_c}{l} + 2\mathcal{H}\right) v d \, d\Omega - \int_\Omega G_c l v \Delta d \, d\Omega = \int_\Omega v 2\mathcal{H} \, d\Omega\,. \tag{26}$$

Applying now the divergence theorem, we obtain

$$\int_\Omega \left(\frac{G_c}{l} + 2\mathcal{H}\right) v d \, d\Omega + \int_\Omega G_c l \nabla v \cdot \nabla d \, d\Omega - \int_{\partial\Omega} G_c l v \nabla d \cdot \mathbf{n} \, d\partial\Omega = \int_\Omega v 2\mathcal{H} \, d\Omega\,. \tag{27}$$

where $\mathbf{n}$ is the exterior normal vector. Splitting now $\partial\Omega = \Gamma_N \cup \Gamma$, where Γ is the Nitsche's boundary, and taking into account that $\nabla d \cdot \mathbf{n} = 0$ on $\Gamma_D \cup \Gamma_N$, we get to the weak form of the problem:

$$\int_\Omega \left(\frac{G_c}{l} + 2\mathcal{H}\right) v d \, d\Omega + \int_\Omega G_c l \nabla v \cdot \nabla d \, d\Omega - \int_\Gamma G_c l v \nabla d \cdot \mathbf{n} \, ds = \int_\Omega v 2\mathcal{H} \, d\Omega\,. \tag{28}$$